Statistical Analysis of ENOB and Yield in Binary Weighted ADCs and DACS With Random Element Mismatch

Jeffrey A. Fredenburg and Michael P. Flynn

***Abstract*—Mismatch motivates many of the design decisions for binary weighted, ratiometric converters, such as successive approximation (SAR) analog-to-digital converters (ADC), but the statistical relationship between mismatch and signal-to-noise-plus-distortion ratio (SNDR) has not been precisely quantified. In this paper, we analyze the effects of capacitor mismatch in a binary weighted, charge redistribution SAR ADC and derive a new analytic expression relating capacitor mismatch and the effective-number-of-bits (ENOB). We then explore the statistics of this new expression and develop a model that accurately predicts yield in terms of ENOB. Finally, the major results of this paper are generalized into a simple and compact design equation that relates resolution, mismatch, and ENOB to yield for all binary weighted, ratiometric converters. The expressions derived in this paper offer practical insight into the relationship between mismatch and performance for all binary, weighted ratiometric converters with these results validated through numerical simulations.**

***Index Terms*—Analog-digital conversion, analog integrated circuits, mismatch, successive approximation registers, yield.**

I. Introduction

SAR ADCs OFFER an attractive solution in low power applications. Due to the inherent energy efficiency of charge redistribution DACs and the leveraged benefits of scaling [1], SAR ADCs can provide power efficient analog to digital conversion in systems that require moderate resolution and speed. However, specific applications have specific needs, and to ensure those needs are met, it is important for designers to have complete understanding of the design tradeoffs in the key building blocks of SAR ADCs, such as the capacitor DAC, the comparator, and the successive approximation registers.

It is well established that mismatch degrades the overall performance of ADCs, and various techniques have been proposed to overcome this degradation [2]–[8]. However, a precise formulation of the relationship between mismatch, the effective number of bits (ENOB), and yield is still lacking. In practice, an ADC designer may need to target a particular ENOB specification, but when estimating the yield, only indirect metrics such as integral nonlinearity (INL) or differential nonlinearity (DNL) are available. Although ENOB, INL, and DNL are important indicators of ADC performance, ENOB is a better indicator of the *overall* system level performance, and with the yield expressions derived in this paper, ADC designers can more easily target system level performance objectives.

The use of INL as a yield metric for data converters is prevalent in literature, but has limited utility in system design. Although the bulk of the analytic work has focused on developing INL yield models for current-steering DACs [9]–[13] in the presence of transistor drain current mismatch [14], the major results of these works are also generally applicable to ADCs. According to [13], the analytical development of INL as a yield metric begins with [9], where the maximum deviation of the INL is introduced as a measure for distinguishing between good and bad current-steering DACs. Later in [10]–[13], we see a progression of refinements aimed towards improving the statistical accuracy of INL based yield estimates. However, none of these works [9]–[13] offer a detailed comparison between INL yield measurements and other performance metrics such as signal-to-noise-plus-distortion ratio (SNDR), and it is unclear how to precisely interpret INL based yield estimates when targeting a specific ENOB yield for ADCs and DACs.

Examples of analysis relating INL/DNL to ENOB can be found in [16]–[18], [24], but these works do not contain a detailed statistical treatment relating ENOB and yield. In [16], DNL is related to signal-to-noise ratio (SNR) by considering DNL errors as an additive noise in flash ADCs. In [17], SNDR is related to INL errors as a function of the input signal probability density function (PDF). In [18], ENOB is related to INL through a harmonic analysis for thermometer-coded structures, and in [24] an approximate relationship between ENOB and INL is given for resistor strings based on analysis in [15]. Although these works provide a convenient sketch relating ENOB and DNL/INL, it is unclear how to extract accurate ENOB yield information.

In this paper, we develop an alternative statistical model using ENOB as a yield metric. First, we examine the effects of mismatch in a binary weighted, charge redistribution SAR ADC. We then derive an exact algebraic formulation relating capacitor mismatch to the average noise power of the ADC output, and from this algebraic formulation, we derive ENOB as a function of capacitor mismatch. Next, we explore the statistics of this ENOB expression and develop a statistical expression that predicts yield in terms of ENOB and mismatch. Finally, we generalize the results of this work by presenting a compact design

Manuscript received March 08, 2011; revised July 19, 2011 and July 19, 2011; accepted October 24, 2011. Date of publication January 16, 2012; date of current version June 22, 2012. This paper was recommended by Associate Editor R. Lotfi.

The authors are with the Department of Electrical Engineering and Computer Science, University of Michigan, Ann Arbor, MI 48109 USA (e-mail: fredenbu@umich.edu).

Digital Object Identifier 10.1109/TCSI.2011.2177006

1549-8328/$31.00 © 2012 IEEE

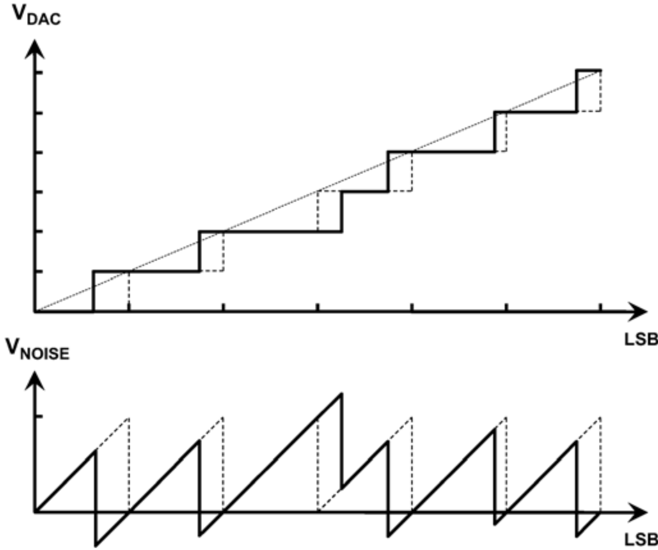

Fig. 1. Transfer function and residual noise voltage of a capacitor DAC with mismatch (solid) and without mismatch (dashed). Without mismatch, the code transitions and DAC outputs occur in regular LSB intervals.

equation, which accurately relates resolution, mismatch, and ENOB to yield for all binary weighted, ratiometric converters. The design equation offered is accurate to within ± 0.17 bits for yield values between 0.5% and 99.5% and is consistent with standard test methodology.

Section II analyzes the effects of mismatch and derives an expression for ENOB as a function of capacitor mismatch. Section III explores the statistics of this ENOB expression, and Section IV formulates an expression for yield. Section V develops a compact design equation for yield, ENOB and mismatch, which generalizes the results of this work.

II. Analytical ENOB Derivation

In this section, we derive an analytic expression for the ENOB of a binary weighted SAR ADC in terms of capacitor mismatch. Although we derive this expression from the perspective of a capacitor DAC, our results are equally valid form the perspective of the ADC. We begin this derivation by relating the INL errors of a DAC to its average noise power. Next, we formulate an expression for the INL in terms of capacitor mismatch parameters, and use this relationship to express the mismatch induced noise power as a function of the capacitor mismatch. Finally, we translate the mismatch induced noise expression into an analytical expression for ENOB which supports differential sinusoidal signals and is consistent with standard ADC test methodology.

A. Mismatch Induced Noise Power

The relationship between the mismatch induced noise power and INL can be derived in a manner similar to the calculation of ideal quantization noise power. By including INL errors into this calculation, we can capture the noise power contributed from INL errors.[1] Fig. 1 shows the transfer function of a DAC and its corresponding noise voltage with and without INL errors. For an ideal single-ended DAC without mismatch, the established $\mathrm{LSB}^2/12$ quantization noise expression represents the mean-squared value of the output noise voltage [18]. Assuming the DAC output codes are uniformly distributed, we can calculate this quantity as shown in (1) and (2)—where N is the DAC resolution in bits, Λ is the LSB, u is the output noise voltage, and u_0 is the mean output noise voltage.

$$V_{\mathrm{noise}}^2 = \frac{1}{2^N \Lambda} \sum_{i=0}^{2^N-1} \int_0^{\Lambda} (u-u_0)^2 du = \frac{\Lambda^2}{12} \tag{1}$$

$$u_0 = \frac{1}{2^N \Lambda} \sum_{i=0}^{2^N-1} \int_0^{\Lambda} u du \frac{\Lambda}{2}. \tag{2}$$

We incorporate mismatch into this expression by modifying the limits of integration in (1) to include the INL errors of the DAC. Since the i-th code transition voltage of a mismatched DAC is offset from the ideal transition voltage by the INL error of that code, we offset the integration limits in (1) by the INL error as shown in (3)—where Φ_i is the INL error of the i-th code expressed in LSB.

$$V_{\mathrm{noise}}^2 = \frac{1}{2^N \Lambda} \sum_{i=0}^{2^N-1} \int_{\Lambda\Phi_i}^{\Lambda(1+\Phi_{i+1})} \left(u - \frac{\Lambda}{2}\right)^2 du. \tag{3}$$

Evaluating the integral in (3) and simplifying the resulting expression, we obtain an expression for the noise power in terms of the INL, which is given by (4).[2] A more intuitive formulation of (4) is also presented in (5).

$$V_{\mathrm{noise}}^2 = \frac{\Lambda^2}{12} + \frac{\Lambda^2}{2^N} \sum_{i=0}^{2^N-1} \Phi_i^2 \tag{4}$$

$$V_{\mathrm{noise}}^2 = \frac{\Lambda^2}{12} + \Lambda^2 \ \mathrm{Mean}\ (\Phi^2). \tag{5}$$

In the limit of a large N, the contribution from the mismatch induced noise power can be approximated as the variance of the INL as shown in (6).[3]

$$V_{\mathrm{noise}}^2 = \frac{\Lambda^2}{12} + \Lambda^2 \ \mathrm{Var}\ (INL). \tag{6}$$

Expressions (4)–(6) describe the average noise power of a single-ended DAC as the sum of the ideal quantization noise and the mean square of the INL errors. These results are generally applicable to all ADCs and DACs with both fixed quantization levels and uniformly distributed DAC outputs and indicate that nonlinearities in the quantization levels manifest as an additive noise. This conclusion is also suggested in [16] for DNL errors.

B. Analytic Formulation of DNL and INL

We continue by formulating an expression for the noise power contributed by the INL errors as a function of capacitor mismatch. To this end, we first introduce a capacitor mismatch model and then derive expressions for DAC DNL errors in terms of this model. Finally, we convert these DNL expressions into INL expressions and solve for the mean squared INL in terms of the capacitor mismatch parameters.

[1] A related result in [16] expresses the average noise power of a flash ADC to its DNL errors.

[2] The DC power contributed by the INL errors is not removed from (4).

[3] A similar result to (6) is derived in [17] using a probabilistic approach.

We model the mismatch of capacitors within the array as an additive random error—i.e., $C = C_{\rm nom} + \Delta C$, where $C_{\rm nom}$ is the nominal design capacitance and ΔC is a normally distributed random error with zero mean with σ_c^2 variance. Furthermore, we define a mismatch parameter γ to describe the fractional error of each binary weighted capacitor group from its ideal value. Assuming that the capacitors are carefully arranged, we neglect pathological errors and effects from spatial gradients.[4]

The mismatch model is provided in (7)—where 2^N is the total number of capacitors in the array, C_u is the average unit capacitance of the array, C_i is the capacitance of the i-th binary weighted capacitor group, and γ_i is the associated fractional mismatch of the i-th group. In addition, we let $i = N$ represent the MSB, $i = 1$ the LSB, and $i = 0$ the termination capacitor. Note that the effective unit capacitance, C_u, is distinct from the nominal design capacitance, $C_{\rm nom}$.

$$\begin{aligned} C_i &= 2^{i-1} C_u (1+\gamma_i) \\ C_u &= \frac{1}{2^N} \sum_{j=1}^{2^N} (C_{\rm nom} + \Delta C_j). \end{aligned} \tag{7}$$

Since the sum of the binary weighted capacitors, defined in (7) as C_i, must equal the total capacitance of the array, the weighted sum of the fractional mismatch parameters γ_i must sum to zero. This condition is enforced by (8).[5]

$$\gamma_0 + \sum_{i=1}^{N} 2^{i-1} \gamma_i = 0. \tag{8}$$

Using the capacitor mismatch model defined in (7) and (8), we now relate the DNL errors of the DAC to the fractional mismatch parameter γ_i. The DNL error of a DAC can be expressed by (9)—where $\Delta V_{\rm DAC}$ is the difference between successive DAC output voltages [19].

$$DNL = \frac{\Delta V_{\rm DAC} - LSB}{LSB}. \tag{9}$$

Furthermore, we can express the DAC output voltages in terms of the binary weighted capacitors as shown in (10)—where N is the resolution in bits, Λ is the LSB, C_i is the i-th binary weighted capacitor group, and $b_i \in \{0,1\}$ represents the digital bits in the DAC code.

$$V_{\rm DAC} = \sum_{i=1}^{N} \frac{b_i C_i}{C_u} \Lambda. \tag{10}$$

Substituting the expression for C_i from (7) into (10), we relate the DAC output voltage to the fractional mismatch parameter γ_i as in (11).

$$V_{\rm DAC} = \sum_{i=1}^{N} b_i 2^{i-1} (1+\gamma_i) \Lambda. \tag{11}$$

[4]An analysis relating INL errors to spatial gradients is found in [20].

[5]Although based on the physical construction of the capacitor array, the constraint on γ given by (8) also ensures that gain errors in the transfer curve are not counted as distortion since (8) imposes a unity gain for the DAC transfer curve.

Using the DAC output voltage expression in (11) and the definition for DNL given in (9), we calculate the DNL errors for each of the 2^N DAC codes. For an N bit, single-ended, binary weighted capacitor DAC, however, the DNL errors are uniquely determined by N distinct DNL values, and these N values represent the DNL error at the major code transitions—specifically, codes 2^{i-1} where $i \in \{1, \ldots, N\}$.

Intuitively, we can understand why the DAC has only N unique DNL by examining the odd numbered codes. Since all the odd numbered codes have a binary representation ending in one, the difference in the DAC output voltage between these codes and one code less is determined solely by the DAC LSB capacitor. Therefore, the DNL error for every odd code is the same and is equal to the DNL error for code 2°, which is an odd code. Using similar examples, we can show through induction that only N unique values are needed to describe the entire DNL of the DAC and these unique values are equal to the DNL at the major code transitions.

We now calculate the DNL errors at the major code transitions by substituting (11) into (9)—where $\Delta V_{\rm DAC}$ from (9) is the difference in the DAC output voltages between codes 2^{i-1} and $2^{i-1} - 1$. An expression for the N unique DNL values is provided in (12)—where d_i represents the DNL error at code 2^{i-1}, and $i \in \{1, \ldots, N\}$.

$$d_i = 2^{i-1} \gamma_i - \sum_{j=1}^{i-1} 2^{j-1} \gamma_j. \tag{12}$$

The distribution of the DNL values given in (12) across each of the DAC codes can be described by the recursively ordered set shown in (13)—where D_N is ordered set of DNL values, and d_N, as described by (12), represents the DNL at the most significant code in the level of hierarchy. The arrangement of DNL values given by (13) describes a sequence in which the N unique DNL values are distributed across the DAC codes in an "x modulo 2^{N-1}" manner.

$$D_N = \{D_{N-1}\ d_N\ D_{N-1}\}. \tag{13}$$

As an example of how (13) describes the DNL distribution, we consider a 3 bit DAC. For $N = 3$, the arrangement of the DNL errors for this DAC is shown in (14)—where d_i is again described by (12).

$$D_3 = \{d_1\ d_2\ d_1\ d_3\ d_1\ d_2\ d_1\}. \tag{14}$$

With both the DNL values and their arrangement calculated, we now relate the INL to the DNL and work towards expressing the mean-squared INL in terms of the mismatch parameter γ_i. The relationship between INL and DNL is shown in (15) [19]—where Φ_i is the INL error at code i, and δ_j is the DNL error at code j. Furthermore, δ_j assumes one of the values described by (12) in an order determined by (13).

$$\Phi_i = \sum_{j=1}^{i} \delta_j. \tag{15}$$

Substituting the DNL expression from (12) into (15) and simplifying the resulting summation by exploiting the inherent folding symmetry of (13), we derive the mean-squared INL in

terms of the mismatch parameter γ_i. The simplified result is shown in (16).

$$\mathrm{Mean}(\Phi^2) = \frac{1}{4}\gamma_0^2 + \frac{1}{4}\sum_{i=1}^{N}\left(2^{i-1}\gamma_i\right)^2. \tag{16}$$

Substituting this expression for the INL noise power from (16) into the noise power expression from (5), we obtain an explicit expression for the average noise power of an N bit single-ended DAC with capacitor mismatch, which is shown in (17)—where Λ is the LSB, and γ_i is the fractional mismatch of the i-th capacitor group as defined in (7). Furthermore, we let $i = N$ represent the MSB, $i = 1$ the LSB, and $i = 0$ the termination capacitor.

$$V_{\mathrm{noise}}^2 = \frac{\Lambda^2}{12} + \frac{\Lambda^2}{4}\left[\gamma_0^2 + \sum_{i=1}^{N}\left(2^{i-1}\gamma_i\right)^2\right]. \tag{17}$$

The expression given in (17) describes the average noise power of a binary weighted DAC as the sum of the ideal quantization noise and a linear combination of the γ_i mismatch parameters squared. Similar to INL and DNL, the mismatch parameter γ_i manifests as additive noise.

C. *Differential Conversion*

Since most high-performance SAR ADCs process differential signals, we now convert the noise power expression given by (17) from a single-ended result into a differential result. If we imagine constructing an N bit, differential DAC using two $N - 1$ bit, single-ended DACs, each with identical mismatch and opposite polarity,[6] the average noise power of this composite differential DAC is the average of the two single-ended DAC noise powers. Using the results from (17) to describe the noise powers of the two $N - 1$ bit single-ended DACs and averaging, we obtain the noise power of an N bit, differential, binary weighted DAC as given in (18)—where Λ now describes the differential LSB, γ_i is the composite fractional mismatch of the i-th capacitor groups, and $\gamma_{i,p}$ and $\gamma_{i,m}$ are the individual mismatch parameters from the positive and negative arrays.

$$\begin{aligned} V_{\mathrm{noise}}^2 &= \frac{\Lambda^2}{12} + \frac{\Lambda^2}{4}\left[\gamma_0^2 + \sum_{i=1}^{N-1}\left(2^{i-1}\gamma_i\right)^2\right] \\ \gamma_i &= \frac{1}{2}(\gamma_{i,p} + \gamma_{i,m}) \quad i \in \{0, \ldots, N-1\} \end{aligned} \tag{18}$$

Equation (18) presents an exact algebraic solution for the average noise power of a binary weighted N bit, differential DAC with uniformly distributed INL errors. Furthermore, since the differential DAC output voltages are perfectly symmetrical about the origin, the noise power given by (18) is zero mean. Additionally, the constraint on γ_i given by (8) properly accounts for gain errors throughout the development of (18).

D. *Analytic Formulation of ENOB*

We now formulate an expression for ENOB in terms of the mismatch parameter γ_i. For a perfectly matched DAC, only the quantization errors contribute noise and the average noise power is $\mathrm{LSB}^2/12$, as shown in (1). If we define an effective LSB size, which generates an average noise power equivalent to the noise power of a mismatched DAC, we can explicitly relate ENOB to the average noise power of the mismatched DAC as is done in (19)—where V_{FS} is the differential full scale range of the DAC output voltage, and Λ_{eff} is the effective LSB size.

$$\begin{aligned} V_{\mathrm{noise}}^2 &= \frac{\Lambda_{\mathrm{eff}}^2}{12} \\ \Lambda_{\mathrm{eff}} &= V_{\mathrm{FS}} \cdot 2^{-\mathrm{ENOB}}. \end{aligned} \tag{19}$$

Substituting the differential noise expression from (18) into (19), we can relate the ENOB of the DAC to the mismatch parameters γ_i. Solving this resulting expression for ENOB, we obtain (20).

$$\begin{aligned} \mathrm{ENOB} &= N - \log_4\left[1 + 3\gamma_0^2 + 3\sum_{i=1}^{N-1}\left(2^{i-1}\gamma_i\right)^2\right] \\ \gamma_i &= \frac{1}{2}(\gamma_{i,p} + \gamma_{i,m}) \quad i \in \{0, \ldots, N-1\}. \end{aligned} \tag{20}$$

Equation (20) offers an exact analytic expression relating the ENOB of an N bit, differential, binary weighted capacitor DAC to capacitor mismatch for uniformly distributed signals. Although we derived (20) from the perspective of a SAR ADC, the result provided in (20) is applicable to all binary weighted ratiometric converters.[7]

E. *Correction for Sinusoidal Distributions*

The ENOB expression given in (20) assumes that the DAC codes are uniformly distributed. In practice, however, the ENOB of an ADC is typically measured using a sinusoidal input signal, not a uniformly distributed signal. With a full-scale, uniformly distributed signal, all of the INL errors across the entire code range each contribute equally to noise. On the other hand, since sinusoidal signals tend to dwell more near their peaks than their mean, the INL errors at the outer codes contribute a larger fraction of the noise than the INL errors near the center codes. Therefore, the noise power contributed by INL errors depends on the probability distribution of the signal.[8]

To reconcile the ENOB expression in (20) with this preferred sinusoidal testing method, we introduce the scalar correction factor, α, to convert the ENOB expression given by (20) into an equivalent expression describing the ENOB of a sinusoidally distributed input signal. The modified ENOB expression is given in (21)—where γ_i represents the composite fractional mismatch parameter of the binary weighted capacitor groups as defined in (18) and (7), and α is approximated as the ratio

[6]This DAC structure represents a generic sign/magnitude encoded structure utilizing a fixed common-mode output.

[7]For binary weighted ratiometric converter without an explicit termination element, γ_0 is still defined as in (8), but should instead be interpreted as either the mean of the single-ended INL errors or a description of the INL induced gain error of the converter transfer function.

[8]If the INL error were constant across the code range, the INL induced noise power would be independent of the signal distribution. This is why the quantization noise does not need to be scaled. By definition, however, the INL errors across an extended code range must sum to zero and therefore cannot remain constant across the codes.

between the INL noise contributions from a sinusoidal distribution and a uniform distribution.[9] A derivation for the estimated value of α used in (21) is offered in Appendix I.

$$\mathrm{ENOB} = N - \log_4\left[1 + 3\alpha\gamma_0^2 + 3\alpha\sum_{i=1}^{N-1}\left(2^{i-1}\gamma_i\right)^2\right]$$
$$\alpha = \frac{3(4-\pi)}{\pi} \cong 0.8197. \quad (21)$$

Equation (21) provides an accurate estimate for the ENOB of N bit, differential, binary weighted ratiometric converters, which is consistent with the standard sinusoidal testing of the ADCs and DACs. Had we not introduced the correction factor α, the ENOB expression would overestimate the mismatch induced noise power by 18%.[10] Using (21), we can now accurately estimate the ENOB of a sinusoidal distribution over a wide range of γ_i values and compare results with standard ADC and DAC test measurements.

III. Statistical ENOB Derivation

Section II provides an analytic expression relating ENOB and mismatch (21), and in this section, we examine the statistics of this ENOB expression. First, we derive the probability density functions (PDF) for the single-ended mismatch parameters $\gamma_{i,p}$ and $\gamma_{i,m}$. Next, we use these PDFs for $\gamma_{i,p}$ and $\gamma_{i,m}$ to derive the PDF for the differential, composite parameter γ_i, and subsequently, the PDF for the square of γ_i. Finally, we combine these results with the ENOB expression given by (21) and obtain a statistical expression for ENOB. Finally, we compare this expression to results from numerical ADC simulations.

A. PDF for the Single-Ended Mismatch Parameter γ

In the capacitor mismatch model presented in (7), each capacitor is modeled as $C = C_{\mathrm{nom}} + \Delta C$, where C_{nom} is the nominal design capacitance and ΔC is a normally distributed error with zero mean with σ_c^2 variance. The PDF for C is shown in (22)—where the PDF is expressed using the notation $\mathrm{f_C}(c)$.

$$\mathrm{f_C}(c) = \frac{1}{\sqrt{2\pi}\sigma_c}\exp\left[\frac{-\left(c - C_{\mathrm{nom}}\right)^2}{2\sigma_c^2}\right]. \quad (22)$$

Furthermore, both the binary weighted capacitor groups and the total array capacitance can be represented as sums of the individual capacitors. Since the sum of independent normal random variables is itself normal with a mean and variance equal to the sum of the constituent means and variances, we obtain the marginal PDFs for the binary weighted capacitors directly from (22) as given in (23)—where N_s is the single-ended resolution, and X_i is the capacitance of the i-th binary weighted capacitor group in one of the single-ended arrays. To avoid parametric equations, we will omit the PDF of the termination capacitor and note that the distribution for the termination capacitor, X_0, follows the same distribution as the LSB capacitor, X_1.

$$\mathrm{f_{X_i}}(x) = \frac{1}{\sqrt{2\pi}\sigma_i}\exp\left[\frac{-(x-\mu_i)^2}{2\sigma_i^2}\right]$$
$$\mu_i = 2^{i-1}C_{\mathrm{nom}} \quad i \in \{1,\ldots,Ns\}$$
$$\sigma_i^2 = 2^{i-1}\sigma_c^2. \quad (23)$$

Similarly, we derive the PDF for the total single-ended array capacitance from (22) as shown in (24)—where N_s is the single-ended resolution, and W is the total capacitance for one of the single-ended arrays.

$$\mathrm{f_W}(w) = \frac{1}{\sqrt{2\pi}\sigma_W}\exp\left[\frac{-(w-\mu_w)^2}{2\sigma_w^2}\right]$$
$$\mu_w = 2^{Ns}C_{\mathrm{nom}}$$
$$\sigma_w^2 = 2^{Ns}\sigma_c^2. \quad (24)$$

Using the definition of γ_i from the mismatch model given in (7), we next reformulate γ_i in terms of the new variables X_i and W as shown in (25). For convenience, we will denote the single-ended fractional mismatch parameter with γ_i. When we derive the composite mismatch parameter, we will clarify the notation with $\gamma_{i,p}$ and $\gamma_{i,m}$.

$$\gamma_i = 2^{Ns+1-i}\frac{X_i}{W} - 1. \quad (25)$$

As shown in (25), the PDF for γ_i is determined by ratio of two *dependent* normal variables, X_i and W, which results in a prohibitively complicated expression for the PDF.[11] In order to simplify this PDF into a form amenable to further analysis, we will therefore expand (25) and approximate the capacitance of the array, W, as a constant in the denominator. The expansion of (25) is given by (26) with W approximated as $2^{Ns}C_u$ in the denominator[12]—where C_u is the mean capacitance of the array as defined in (7).

$$\gamma_i = \frac{2^{Ns+1-i}X_i - W}{2^{Ns}C_u}. \quad (26)$$

Using the PDFs for X_i and W from (23) and (24), we now derive an approximation of the marginal PDF for γ_i through the expansion given by (26). The simplified PDF for γ_i is provided in (27)—note that the correlation between X_i and W in the numerator has not been neglected.

$$f_{\Gamma_i}(\gamma) \cong \frac{1}{\sqrt{2\pi}\sigma_i}\exp\left[\frac{-\gamma^2}{2\sigma_i^2}\right]$$
$$\sigma_i^2 \cong \left[2^{1-i} - 2^{-Ns}\right]\left[\frac{\sigma_c}{C_{\mathrm{nom}}}\right]^2 \quad i \in \{1,\ldots,Ns\}. \quad (27)$$

We now calculate the PDF for the composite mismatch factor. Using (27) to describe the distributions for $\gamma_{i,p}$ and $\gamma_{i,m}$, we obtain the PDF for composite mismatch factor using the relationship for the mismatch factors given by (20), which states that the

[9]Alternatively, the ENOB of sinusoidally distributed DAC codes can be derived by replacing the "averaging" in (3) with the probability mass function (PMF) of a sinusoidal distribution, but it is unclear whether a tractable ENOB expression can be obtained due to the complexity of the sinusoidal PMF.

[10]Since α linearly scales only the mismatch induced noise power, the 18% overestimation can be approximated by $1 - \alpha$.

[11]An exact formulation of this PDF is derived in [15] to analyze nonlinearities in resistor strings.

[12]Approximating W as $2^{\mathrm{Ns}}\mathrm{Cu}$ follows from the weak law of large numbers and is equivalent to assuming that $\sigma_c/\mathrm{C_{nom}}$ is well approximated by $\sigma_c/\mathrm{C_u}$ when the number of capacitors is large.

composite mismatch factor is the average of the single-ended mismatch factors. The PDF for the composite mismatch factor is provided in (28)—where N is the differential resolution and is related to single-ended resolution,[13] Ns, by $N = Ns + 1$.

$$f_{\Gamma_i}(\gamma) \cong \frac{1}{\sqrt{2\pi}\sigma_i} \exp\left[\frac{-\gamma^2}{2\sigma_i^2}\right]$$
$$\sigma_i^2 \cong [2^{-i} - 2^{-N}] \left[\frac{\sigma_c}{C_{\text{nom}}}\right]^2 \quad i \in \{1, \ldots, N1\}. \quad (28)$$

Equation (28) provides an analytic expression for the PDF of the composite mismatch parameter γ_i of an N bit differential DAC—where γ_0 follows the same distribution as γ_1.

B. Statistical ENOB Expression

Since the ENOB expression in (21) depends on a linear combination of γ_i^2, we now derive the PDF for the square of the composite mismatch factor from the PDF of the composite mismatch factor. Letting $\eta_i = \beta_i \gamma_i^2$—where β_i represents the scalar coefficients from the ENOB expression given by (21), the PDF of η_i follows a Chi-Squared distribution [21]. Using the PDF described from (28) and replacing the scalars β_i with the appropriate values from (21), we calculate the distribution for η_i, which is shown in (29)[14]—where the distributions for η_0 is described by the distribution for η_1.

$$f_{\text{H}_i}(\eta) \cong \frac{1}{\sqrt{2\pi}\sigma_i} \eta^{-1/2} \exp\left[\frac{-\eta}{2\sigma_i^2}\right]$$
$$\sigma_i^2 \cong \frac{9(4-\pi)}{4\pi} [2^i - 2^{2i-N}] \left[\frac{\sigma_c}{C_{\text{nom}}}\right]^2 i \in \{1, \ldots, N-1\}. \quad (29)$$

Substituting η_i into the ENOB expression (21), we express the ENOB in terms of η_i as shown in (30)—where the distributions for η_i are described in (29).

$$\text{ENOB} = N - \log_4 \left[1 + \sum_{i=0}^{N-1} \eta_i\right]. \quad (30)$$

Equation (30) provides an analytic model describing the statistics for the ENOB of an N bit, binary weighted, differential SAR ADC with a normally distributed capacitor mismatch. Furthermore, this model includes a sinusoidal correction factor, so this statistical model is valid for sinusoidally distributed signals and is thus compatible with standard ADC test methods.

C. Expected Value and Variance

We verify the validity of (30) by comparing analytical expressions for the expected value and variance of ENOB to numerical simulations of randomly generated SAR ADCs. Because the ENOB expression in (30) contains a logarithmic term, we will estimate the expected value and variance using a Taylor series expansion.

[13]This DAC structure represents the generic sign/magnitude encoded structure described in II-C which utilizes a fixed common-mode output.

[14]This PDF is an approximation for the marginal PDF for η.

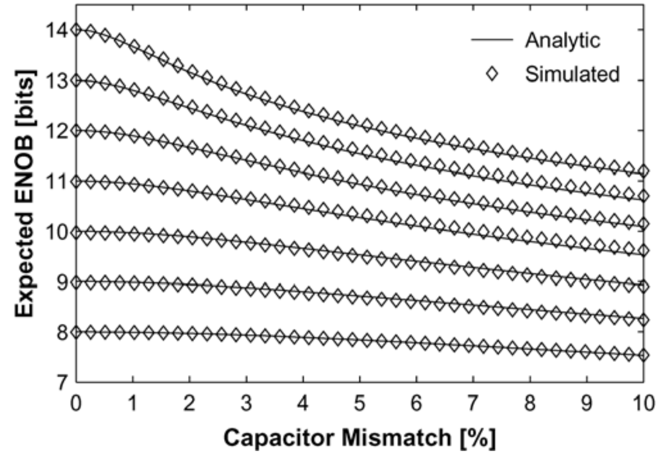

Fig. 2. Comparison between simulated and calculated expected values (32) for ENOB across various resolutions. The numerical simulation results are obtained using a 1024 point FFT of 300,000 randomly mismatched ADCs at each resolution and each standard deviation of capacitor mismatch.

Letting X represent the sum of η_i in (30), the Taylor series expansion for the ENOB centered at $\text{E}[X]$ is shown in (31).

$$\text{ENOB} = N - \log_4 (1 + \text{E}[X]) - \sum_{k=1}^{\infty} \frac{(-1)^k}{k! \ln 4} \left(\frac{X - \text{E}[X]}{1 + \text{E}[X]}\right)^k. \quad (31)$$

Taking the expected value of (31) and dropping higher order terms, we obtain the approximation for the expected ENOB shown in (32).

$$\text{E[ENOB]} = N - \log_4 (1 + \text{E}[X]) + \frac{\text{Var}[X]}{2 \ln 4 (1 + \text{E}[X])^2}. \quad (32)$$

Due to the complexity of including correlations between each η_i in later analysis, we will neglect all correlations.[15] Therefore, treating the η_i from (30) as independent variables, we can approximate the expected value and variance of X as the sum of the expected values and variances of η_i. Figs. 2 and 3 offer a comparison between the calculated and simulated values for the expected ENOB of a SAR ADC. As shown in Fig. 2, the calculated ENOB values track the simulated values reasonably well, and in Fig. 3, we see that the analytic expected value is within 1.0% of the simulated value over a wide range of resolution and mismatch.[16]

Next, we obtain an expression for the ENOB variance. Taking the variance of (31) and dropping higher order terms, we derive (33).

$$\text{Var[ENOB]} = \frac{\text{Var}[X]}{[\ln 4 (1 + \text{E}[X])]^2}. \quad (33)$$

[15]A comparison between the first four moments of the ENOB expression given in (30) and the moments calculated from simulation data showed reasonable similarity, which included correlations, and the moments derived from (30) with η_i treated as independent random variables.

[16]In Fig. 3, however, the error in the expected ENOB is non-monotonic with respect to resolution, we attribute this to the fixed 1024 point FFTs used to generate the simulation data. With a fixed 1024 FFT, only a subset of the output codes is measured for resolutions beyond 11 bits.

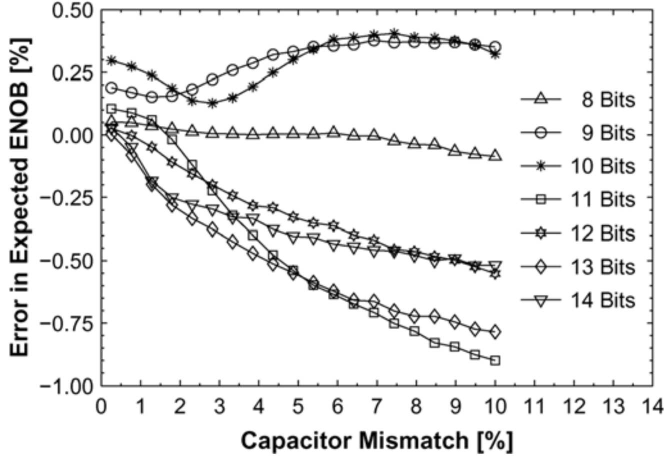

Fig. 3. Comparison between simulated and calculated expected values (32) for ENOB across various resolutions expressed as percent error. The analytic expected ENOB values are within $\pm 1.0\%$ of simulated values.

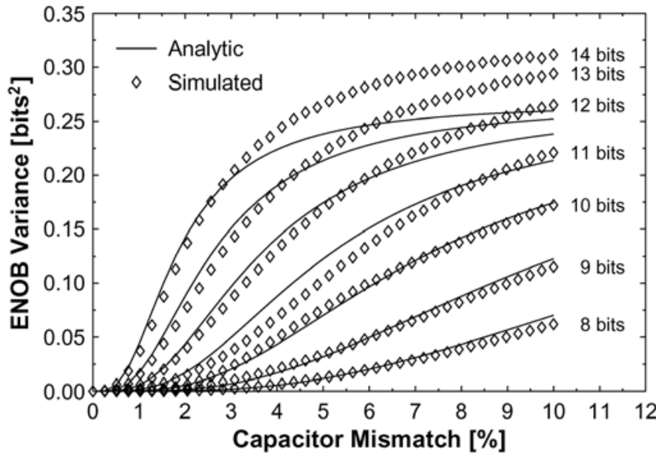

Fig. 4. Comparison between the simulated and calculated ENOB variances (33) across various resolutions. The numerical simulation results are obtained using a 1024 point FFT of 300,000 randomly mismatched ADCs at each resolution and each standard deviation of capacitor mismatch.

Similar to the expected value calculation, we treat the η_i from (30) as independent variables and approximate the variance of X as the sum of the η_i variances. Fig. 4 compares the calculated and simulated values for the ENOB variance.

As shown in Fig. 4, the calculated variances compress at higher resolutions. This compression indicates a nonlinear relationship between the calculated and simulated variances. Since the inclusion of higher order terms up to the fourth moment of X in the Taylor series expansion did not reduce this error, we attribute the causes of this discrepancy to the scalar correction factor, α, and the assumption that the η_i are independent. While the correction factor α correctly scales the expected ENOB to approximate a sinusoidal distribution, α does not properly scale the higher moments. Furthermore, the η_i are not independent since the γ_i mismatch parameters are correlated, which is evidenced by (8). Nevertheless, the magnitude of the error between the calculated and simulated variances is small compared to the resolution of the ADC.

IV. Yield Analysis

We complete the statistical analysis of ENOB with an examination of the ENOB yield for an N bit, binary weighted, differential SAR ADC. Using the ENOB expression given in (30), we can express the probability of achieving some minimal ENOB in terms of the probabilities for η_i as shown in (34)—where $\mathrm{ENOB_{MIN}}$ is the minimal desired ENOB, and N is the ADC resolution in bits.

$$\mathrm{P}(\mathrm{ENOB} > \mathrm{ENOB_{MIN}}) = \mathrm{P}(X < 4^{N-\mathrm{ENOB_{MIN}}} - 1)$$
$$X = \sum_{i=0}^{N-1} \eta_i. \tag{34}$$

A. Full Yield Approximation

We next derive an approximate ENOB yield expression in terms of the cumulative distribution function (CDF) for X from (34). The details of this derivation are provided in Appendix II.

When N is even number of bits, the CDF of X can be approximated as in (35)—where $\mathrm{F_X(x)}$ denotes the CDF of X, $\sigma_{2\mathrm{i}-2}$ is the i-th even σ from (29) including σ_0, $\sigma_{2\mathrm{i}-1}$ is i-th odd σ from (29), and $\sigma_{\mathrm{N}-1}$ denotes the value in the sequence.

$$\mathrm{F_X}(x) = \int_0^x \int_0^{\frac{\pi}{2}} \cdots \int_0^{\frac{\pi}{2}} \sum_{i=1}^{N/2} B_i e^{-\lambda_i t} d\theta_1 \cdots d\theta_{N/2} dt$$
$$B_i = \left[(\lambda_i - s) \prod_{j=1}^{N/2} \left(\frac{A_j}{\lambda_j - s} \right) \right|_{s \to \lambda_i}$$
$$A_i = \frac{1}{\pi \sigma_{2i-2} \sigma_{2i-1}} \quad \lambda_i = \frac{\cos^2 \theta_i}{2\sigma_{2i-2}^2} + \frac{\sin^2 \theta_i}{2\sigma_{2i-1}^2}. \tag{35}$$

When N is odd number of bits, the CDF of X can be approximated as in (36)—where, again, where $\mathrm{F_X(x)}$ denotes the CDF of X, $\sigma_{2\mathrm{i}-2}$ is the i-th even σ from (29) including σ_0, $\sigma_{2\mathrm{i}-1}$ is i-th odd σ from (29), and $\sigma_{\mathrm{N}-1}$ denotes the last value from (29).

$$\mathrm{F_X}(x) = \int_0^x \int_0^{\frac{\pi}{2}} \cdots \int_0^{\frac{\pi}{2}} \sum_{i=1}^{N/2} C_i e^{-\omega_i t} d\theta_1 \cdots d\theta_{N/2} d\varphi dt$$
$$B_i = \left[(\lambda_i - s) \prod_{j=1}^{N/2} \left(\frac{A_j}{\lambda_j - s} \right) \right|_{s \to \lambda_i}$$
$$A_i = \frac{1}{\pi \sigma_{2i-2} \sigma_{2i-1}} \quad \lambda_i = \frac{\cos^2 \theta_i}{2\sigma_{2i-2}^2} + \frac{\sin^2 \theta_i}{2\sigma_{2i-1}^2}$$
$$C_i = B_i \sin\varphi \sqrt{\frac{2t}{\pi \sigma_{N-1}^2}} \quad \omega_i = \lambda_i \sin\varphi + \frac{\cos^2 \varphi}{2\sigma_{N-1}^2}. \tag{36}$$

Using the ENOB relationship given by (34) along with the CDFs provided by (35) and (36), we can now calculate the ENOB yield for an N bit, binary weighted, differential SAR ADC, but due to the complexity of these equations, however, we provide a more convenient approximation Section V.

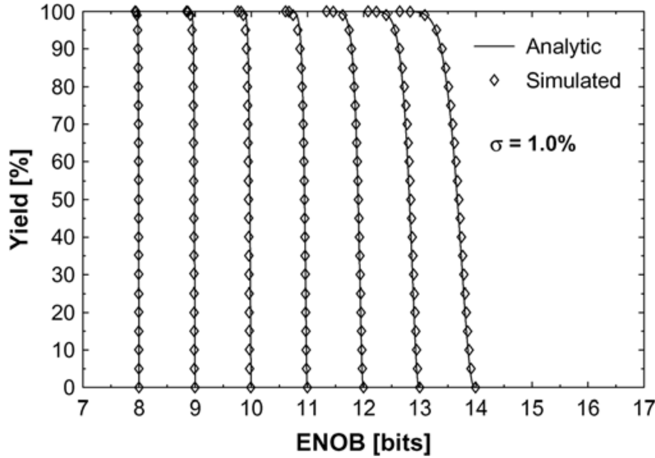

Fig. 5. Comparison between the simulated and analytic ENOB yields with a standard deviation of 1.0% capacitor mismatch.

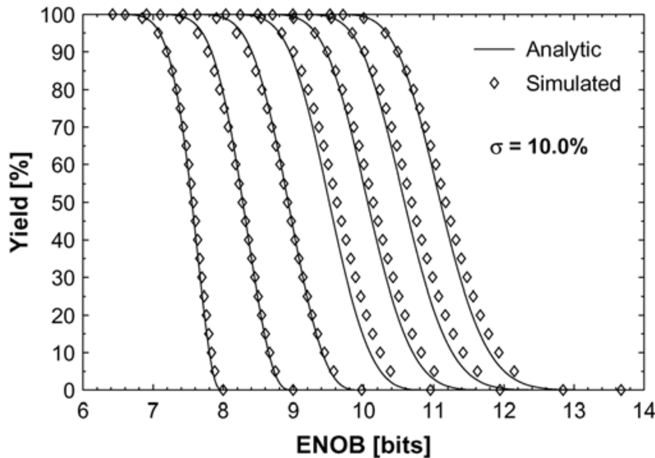

Fig. 6. Comparison between the simulated and analytic ENOB yields with a standard deviation of 10% capacitor mismatch.

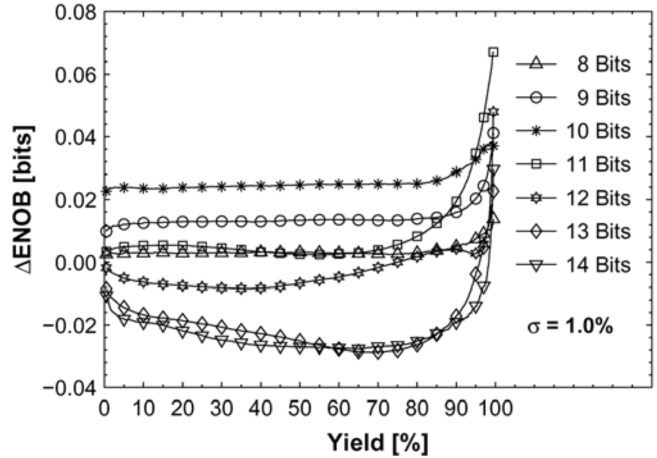

Fig. 7. Error between the simulated and analytical ENOB values as a function of the yield for a 1% standard deviation of capacitor mismatch. The absolute error in the ENOB is within ± 0.08 bits over the range of yields from 0.5% to 99.5%.

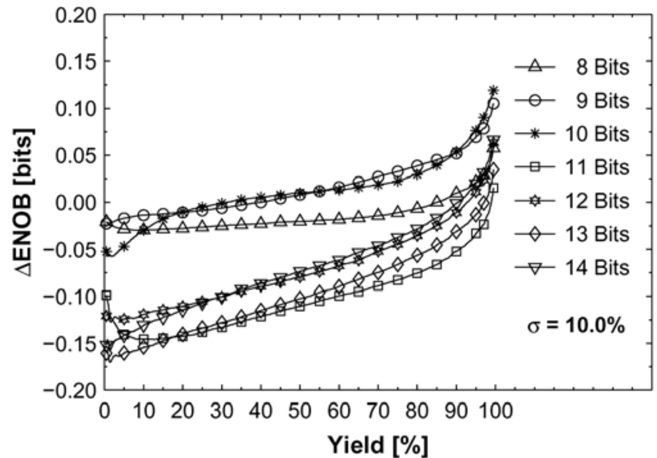

Fig. 8. Error between the simulated and analytical ENOB values as a function of the yield for a 10% standard deviation of capacitor mismatch. The absolute error in the ENOB is within ± 0.17 bits over the range of yields from 0.5% to 99.5%.

B. Comparison With Simulation Results

We now compare the ENOB yields predicted by the analytic expression for the CDF of X provided in (35) and (36) to simulated ENOB values. The simulated ENOB yield values are obtained using a 1024 point FFT with a sample of 300,000 randomly mismatched SAR ADCs generated at each resolution and each standard deviation of mismatch. Furthermore, the yield values are extracted from histograms of simulated ENOB values over uniformly distributed bins.

In Figs. 5 and 6, we compare the analytic and simulated ENOB yield curves for capacitor mismatch standard deviations of 1% and 10%. At 1% mismatch, Fig. 5, we see excellent agreement between the analytic and simulated yield curves, but at 10% mismatch, Fig. 6, we notice some difference between the analytical and simulated yield curves. Although the 8–10 bits yield curves from Fig. 6 match well, the 11–14 bit curves display a larger divergence at lower yield values.

Figs. 7 and 8 offer a more detailed comparison between the analytic and simulated yield curves provided in Figs. 5 and 6. As shown in Fig. 7, the error between the simulated and analytic ENOB values at 1% mismatch is within ± 0.08 bits for 8–14 bits of resolution across the range of yields between 0.5%–99.5%. In Fig. 8, the error in the ENOB at 10% mismatch is within ± 0.17 bits across the range of yields between 0.5%–99.5%. Therefore, at a particular yield value, we see an error in the predicted ENOB less than ± 0.08 bits at 1% mismatch and less than ± 0.17 bits at 10% mismatch.

In Figs. 7 and 8, we see that the largest errors in the ENOB occur as the yield approaches 0% and 100%. We attribute the source of this error to correlations between η_i values. Since the γ_i mismatch parameters are correlated, which is shown in (8), the η_i values are correlated as well. By neglecting these correlations in our statistical model, the frequency of outliers at the tails of the CDF curves are underestimated. Nevertheless, the error in the predicted ENOB is relatively small and the expressions for the CDF of X given in (35) and (36) offer a reasonably accurate estimate for the ENOB yield of SAR ADCs and, in general, all binary weighted ratiometric converters.

V. Simplified Yield Expression

The ENOB yield model provided by (34)–(36) from Section IV expresses the yield as a function of sigma mismatch and bit resolution. These equations, however, are computationally expensive and cannot be inverted to calculate mismatch as

a function of the yield. In this section, we therefore offer an accurate, yet simple, approximation for these expressions which are invertible and allow both the bit resolution and capacitor mismatch to be represented as functions of the ENOB yield.

In what follows, we first develop a single design equation that relates the yield, capacitor mismatch, ENOB, and bit resolution in a more convenient form than (35) and (36). We then present a sample calculation showing how to extract desired parameters from this new yield expression. Finally, we conclude this section by comparing this compact yield expression to both simulation results and the full expressions derived in Section V.

A. Formulation of Simplified Yield Expression

In (34), we express the probability of maintaining some minimal ENOB as a function X, where X is defined as a sum of Chi-Squared random variables with marginal PDFs described by (29). Since the sum of independent and identically distributed (iid) Chi-squared random variables follows a Gamma distribution, we standardize X in terms of mismatch and bit resolution and approximate its standardized CDF with a normalized incomplete Gamma function, which is the analytic form of the CDF for sums of iid Chi-squared variables. The standardization of X is provided in (37) and the form of our approximation for the standardized CDF is given in (38)—where Z represents our standardized variable, and $\mathrm{F_Z}(z)$ is the CDF of Z expressed as an incomplete Gamma function. Furthermore, we denote Γ as the Gamma function and let k and b represent the shape and scale parameters of $\mathrm{F_Z}(z)$.

$$Z = X \cdot 2^{-N} \left[\frac{C_{\mathrm{nom}}}{\sigma_{\mathrm{c}}}\right]^2 \tag{37}$$

$$\mathrm{F_Z}(z) = \frac{1}{\Gamma(k)} \int_0^{b\sqrt{z}} t^{k-1} e^{-t} dt. \tag{38}$$

Using numerical optimization, we calculate values for k and b which minimize the error between the CDF given in (38) and standardized forms of the full CDFs given in (35) and (36) across the entire 8–14 bit resolution range. A complete formulation of our simplified yield approximation is given in (39)—where $\mathrm{ENOB_{MIN}}$ is the minimum desired ENOB, N is the resolution in bits, $\sigma_{\mathrm{c}}/C_{\mathrm{nom}}$ is the standard deviation of the fractional mismatch, $\mathrm{F_Z}(z)$ is the CDF of Z as described by (38),[17] Γ is the Gamma function, and both k and b are empirical fitting parameters.

$$\begin{aligned} \mathrm{P}(\mathrm{ENOB} > \mathrm{ENOB_{MIN}}) &= \mathrm{P}(X < 4^{N-\mathrm{ENOB_{MIN}}} - 1) \\ Z &= X \cdot 2^{-N} \left[\frac{C_{\mathrm{nom}}}{\sigma_{\mathrm{c}}}\right]^2 \\ \mathrm{F_Z}(z) &= \frac{1}{\Gamma(k)} \int_0^{b\sqrt{z}} t^{k-1} e^{-t} dt \\ k = 7.944 \quad & b = 13.146. \end{aligned} \tag{39}$$

[17]Both the expressions for $\mathrm{F_Z}(z)$ and its inverse are standard functions in most commercial math programs.

```
% Parameter Values
N = 9;  SIGMA = 0.1;  ENOB_MIN = 7.7;
YIELD = 0.95;  k = 7.944;  b = 13.146;

% Yield Calculation
X=4^(N-ENOB_MIN)-1;
Z=X/2^N/SIGMA^2;
YIELD=gammainc(b*sqrt(Z),k)

% Sigma Calculation
X=4^(N-ENOB_MIN)-1;
Z=(gammaincinv(YIELD,k)/b)^2;
SIMGA=sqrt(X/Z/2^N)
```

Fig. 9. Example MATLAB code for implementing the yield equation provided in (39). This code calculates the yield as function of resolution and mismatch and calculates mismatch as a function of yield and resolution.

Equation (39) relates yield, mismatch, ENOB, and resolution in a single closed form expression. For simplicity, we offer MATLAB code in Fig. 9 as an example of how to interpret (39)—where we have implemented $\mathrm{F_Z}(z)$ using the standard function provided by the software. When this code is executed, the yield calculation will return 95% for YIELD and the sigma calculation will return 0.1 for SIGMA. We omitted the resolution calculation, but this calculation is easily derived from the sigma calculation by rearranging the terms.

B. Comparison of Yield Expression

We now compare the yield expression from (39) to both the full expressions from Section IV and simulation results. In Fig. 10, we plot the difference between yield values calculated using the approximation given in (39) and analytic values calculated using (35) and (36) as standardized to Z through (37). As shown in Fig. 10, the error in the yield values, expressed as a difference in percentages, is within $\pm 0.16\%$ over the range of resolutions between 8–14 bits. This shows that the simplified expression provided by (39) is a good approximation of the full expressions from Section IV.

In Figs. 11 and 12, we compare ENOB values calculated using (39) to simulated values at a constant yield of 95%. The simulated yield values are obtained using a 1024 point FFT with a sample of 300,000 randomly mismatched SAR ADCs generated at each resolution and each standard deviation of mismatch. As shown in Fig. 11, the analytic ENOB values obtained from (39) agree with the simulated values, and as shown in Fig. 12, these analytic ENOB values match within ± 0.12 bits at a constant 95% yield.

Equation (39) represents a simple and accurate design equation for calculating yield. In (39), the CDF of X is standardized and related to a normalized incomplete Gamma function. Since both the incomplete gamma function and its inverse are standard functions in most numerical software packages, (39) provides a convenient design approximation which relates mismatch, ENOB, and yield for binary weighted ratiometric converters.

Although we have neglected losses in ENOB that occur from comparator noise, kT/C noise, and sampling jitter, (39)

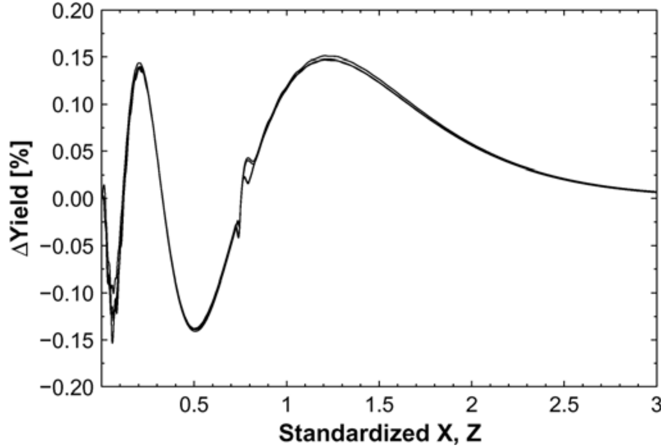

Fig. 10. Error in yield values between (39) and the full expression given by (35) and (36) as standardized to Z through (37) at each resolution from 8–14 bits. The error is expressed as difference in percentages. Since the differences in yields associated with each of the 8–14 bit curves resemble one another so closely, we do not distinguish between the 7 individual curves. As shown, the absolute error between the yield values is within $\pm 0.16\%$ which indicates that the Gamma Distribution approximation from (39) matches the full expressions very well.

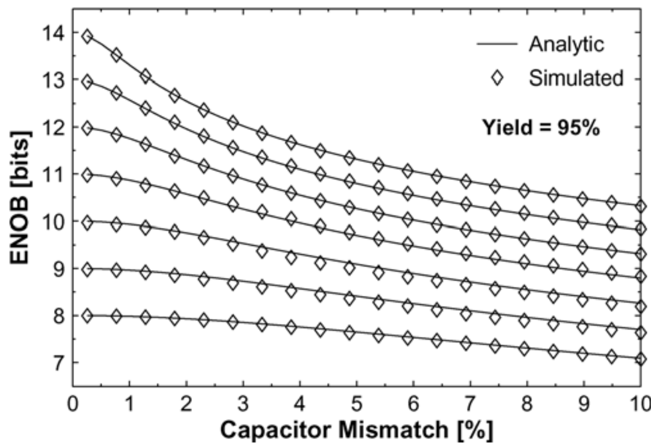

Fig. 11. Comparison between simulated and the analytically calculated ENOBs using the approximation from (39) for a constant yield of 95%. The plot shows the minimum value of ENOB allowed for a good ADC to achieve a yield of 95%. As shown, the simulated values of ENOB match the analytic curves.

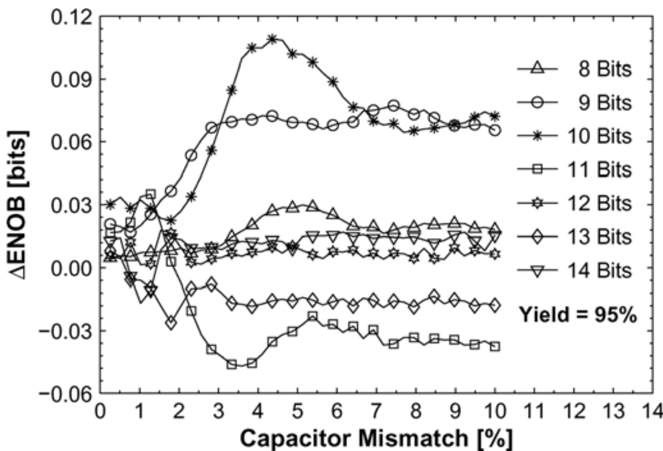

Fig. 12. Error between simulated and analytically calculated ENOBs using the approximation from (39) with a constant yield of 95%. The error between the analytic and simulated ENOBs is less than ± 0.12 bit.

can accommodate a more comprehensive yield analysis using these additional noise sources. Assuming these additional noise sources are independent, we can normalize each of their powers by $\Lambda^2/4$ and add them to X in (34). Once included in X, we can we can calculate a refined ENOB yield equation by convolving the PDFs of the additional noise power terms with the PDF for X.

VI. Conclusions

In this paper, we develop a yield model for binary weighted SAR ADCs based on ENOB which is applicable to all binary weighted ratiometric converters, and we present the results as an accurate and easily implementable design equation. In addition, we derive an exact analytical expression relating mismatch and resolution to ENOB for uniformly distributed signals, and also offer an accurate expression relating mismatch and resolution to ENOB for sinusoidal signals. This work presents the first mathematical expression relating resolution, mismatch, ENOB, and yield. From this work, the mismatch required to achieve a certain ENOB with a particular yield can be calculated, and the fundamental limit on accuracy for binary weighted ratiometric converters can be estimated in terms of component matching.

Appendix I

Correction Factor for Sinusoidal Distributions

In this Appendix, we derive a linear scaling factor α which estimates the noise power contributed by sinusoidal signals in terms of the noise power contributed by uniformly distributed signals. As shown by (4) and (5), the average noise power of a single-ended DAC is expressed as the sum of the quantization noise and the mean squared INL. This noise power formulation suggests that we can obtain the noise power for a sinusoidal distribution by reweighting the mean squared INL values according to the probability mass function of a sinusoidal distribution. In what follows, we first develop an expression for the squared INL values and then use this expression to calculate the average INL noise power contributed by both uniform and sinusoidal DAC code distributions. Finally, we extract the linear scaling factor α from the ratio of these noise powers.

We obtain an analytic formulation of the of the squared INL values by simulating the INL of mismatched differential DACs and numerically calculating the mean squared INL at each code. Fig. 13 graphs the simulated mean square INL values, and (40) provides a quadratic approximation of the results—where Φ_i is the INL at code i, N is the number of bits, and A is the peak amplitude of the squared INL values.

$$\Phi_i^2 = \begin{cases} A\frac{i(2^{N-1}-i)}{2^{2N-4}} & 0 \le i \le 2^{N-1} \\ A\frac{(2^N-i)(i-2^{N-1})}{2^{2N-4}} & 2^{N-1} \le i \le 2^N \end{cases}. \tag{40}$$

To simplify the calculations, we normalize the code range of (40) to half a period. The normalized INL expression is given in (41)—where x is the normalized index variable.

$$\Phi_x^2 = \begin{cases} 4Ax(1-x) & 0 \le x \le 1 \\ 4A(x-1)(2-x) & 1 \le x \le 2 \end{cases}. \tag{41}$$

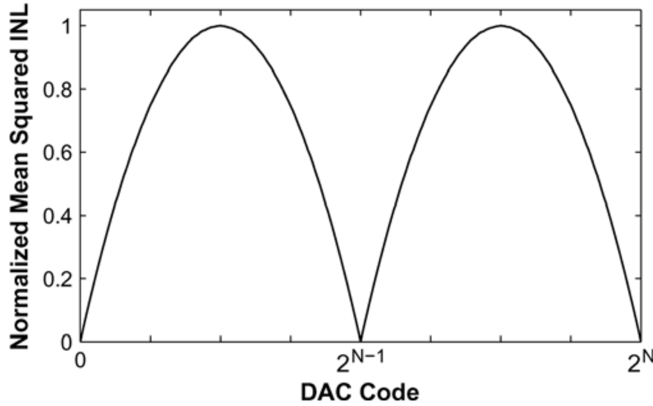

Fig. 13. Simulated values of the normalized mean squared INL at each code of an N bit DAC. The INL values were obtained by averaging the squared INL values at each code across randomly mismatched DACs.

Assuming an infinite resolution DAC with continuously distributed INL values, we estimate the average noise power contributed from uniformly distributed INL errors by integrating (41) across one period of the normalized code range. This calculation is shown in (42).

$$V_{\text{noise,INL}}^2 = 4A\int_0^1 x(1-x)dx = \frac{2A}{3}. \tag{42}$$

Similarly, we calculate the average noise power contributed from sinusoidally distributed INL errors by weighting the squared INL values according to a sinusoidal probability distribution and again integrating across a normalized code range. This calculation is shown in (43).

$$V_{\text{noise,INL}}^2 = \frac{8A}{\pi}\int_0^1 \frac{x(1-x)}{\sqrt{1-x^2}}dx = \frac{2A(4-\pi)}{\pi}. \tag{43}$$

Letting α equal the ratio of these noise contributions, we obtain the estimate for α given in (44).

$$\alpha = \frac{3(4-\pi)}{\pi} \cong 0.8197. \tag{44}$$

With this value for α, we can now estimate the noise power contribution from a sinusoidal signal in terms of a uniformly distributed signal, which enables us to estimate the ENOB of a sinusoidal distribution and compare results with standard ADC test measurements.

Appendix II

Full Yield Approximation—CDF of X Derivation

As shown in (34), the probability of maintaining some minimal ENOB can be expressed as the probability that X remains within some bound determined by the desired ENOB. Therefore, we can estimate the ENOB yield using the cumulative distribution function (CDF) of X. In what follows we will derive the CDF for X and compare the analytic expression for the ENOB yield to simulation results.

Treating the η_i in (34) as independent random variables, we can express the PDF of X as the series convolution of the eta_i PDFs, which are defined in (29). This expression for the PDF for X is shown in (45)—where Π^* denotes the convolution operator.

$$\mathrm{f_X}(x) = \left[\prod *\right]_{i=0}^{N-1} \mathrm{f_{H_i}}(x). \tag{45}$$

To obtain the CDF for X, we must compute the series convolution shown in (45). Although we can efficiently compute this convolution by transforming each of the η_i PDFs into the s domain and multiplying their moment generating functions,[18] the resulting s domain expression we obtain for X is poorly structured and lacks a clear procedure for inverting the transformation and recovering a PDF.[19] Furthermore, a direct numerical calculation of this series convolution is troublesome since the PDFs of η_i are singular at the origin, which leads to numerical instability. In lieu of these difficulties, a less straightforward approach is used to derive a computationally feasible expression for the PDF of X.[20]

The method we employ to derive the CDF of X is based on an s domain transformation over convolved pairs of η_i. First, we will analytically compute the convolution over particular pairs of η_i, and then perform an s domain transformation on these expressions to obtain the moment generating functions. Next, we multiply the resulting moment generating functions and obtain a form for the moment generating function of X which is invertible. Finally, we recover the PDF of X and integrate to obtain the CDF. Following this procedure, we obtain an analytic expression for the CDF of X amenable to numerical approximation using standard numerical integration techniques.

Letting η_{ij} represent the sum of η_i and η_j, we can express the PDF of η_{ij} as the convolution of the η_i and η_j PDFs as in (46)—where σ_i and σ_j are described in (45).

$$\mathrm{f_{H_{ij}}}(\eta) \cong \frac{1}{2\pi\sigma_i\sigma_j}\int_0^\eta \frac{1}{\sqrt{t(\eta-t)}}\exp\left[\frac{-t}{2\sigma_i^2}+\frac{-(\eta-t)}{2\sigma_j^2}\right]dt. \tag{46}$$

Using the trigonometric substitution $t=\eta\cos^2\theta$, we reduce (46) into the alternative formulation shown by (47), which resembles the PDF of an exponential random variable. The integral expression given in (47) represents our final simplification for the PDF of η_{ij}.

$$\mathrm{f_{H_{ij}}}(\eta) \cong \frac{1}{\pi\sigma_i\sigma_j}\int_0^{\frac{\pi}{2}} e^{-\lambda_{ij}\eta}d\theta$$
$$\lambda_{ij} = \frac{\cos^2\theta}{2\sigma_i^2}+\frac{\sin^2\theta}{2\sigma_j^2}. \tag{47}$$

[18]Moment generating functions are analogous to Laplace transformations, where convolutions become products in the s domain.

[19]The moment generating functions for η_i each contain distinct branch points along the real axis.

[20]A simple closed form expression for the CDF of a linear combination of Chi-Squared variables does not exist, but possible alternative computational solutions to this problem can be found in [22], [23], where [22] offers an algorithm for numerically inverting the moment generation function, and [23] presents a asymptotic expansion based on an infinite series of incomplete gamma integrals.

Next, we transform (47) into the s domain by calculating its moment generating function. Since the expression in (47) is absolutely convergent within the region of convergence for s, we can apply Fubini's Theorem and interchange of the order of integration during this transformation. The resulting moment generating function for η_{ij} is shown in (48).

$$\mathrm{M_{H_{ij}}}(s) \cong \frac{1}{\pi\sigma_i\sigma_j}\int_0^{\frac{\pi}{2}} \frac{1}{\lambda_{ij}-s}d\theta$$
$$\lambda_{ij} = \frac{\cos^2\theta}{2\sigma_i^2} + \frac{\sin^2\theta}{2\sigma_j^2}. \tag{48}$$

The expression given in (48) is the moment generating function of the convolution over the pairs η_i and η_j. From a practical perspective, however, the integrand of (48) is just the moment generating function of an exponential random variable. Since moment generating functions formed through products of exponential random variables are easily inverted using Cauchy's Residue Theorem,[21] we can generate an invertible representation for X in the s domain by multiplying the moment generating functions derived from convolved pairs of η_i.

Assuming that the resolution of the ADC is an even number of bits, the number of terms summed in X is even, and we can reduce the series convolution described by (45) into a series product of moment generating functions of the form given by (48). We will address the case where X is the sum of an odd number of terms later. Multiplying each of these moment generating functions, we obtain (49)—where $\mathrm{M_X(x)}$ is the moment generating function of X, i denotes the moment generating function derived from i-th convolved pair of η, σ_{2i-2} is the i-th even σ from (45) including σ_0, and σ_{2i-1} is i-th odd σ from (45).[22]

$$\mathrm{M_X}(s) = \int_0^{\frac{\pi}{2}}\cdots\int_0^{\frac{\pi}{2}}\prod_{i=1}^{N/2}\left(\frac{A_i}{\lambda_i-s}\right)d\theta_1\cdots d\theta_{N/2}$$
$$A_i = \frac{1}{\pi\sigma_{2i-2}\sigma_{2i-1}} \quad \lambda_i = \frac{\cos^2\theta_i}{2\sigma_{2i-2}^2} + \frac{\sin^2\theta_i}{2\sigma_{2i-1}^2}. \tag{49}$$

Using Cauchy's Residue Theorem to invert (48), we recover the PDF of X. Integrating this PDF, we obtain the CDF for X as given in (35)—where σ_{2i-2} is the i-th even σ from (45) including σ_0, σ_{2i-1} is i-th odd σ from (45).

$$\mathrm{F_X}(x) = \int_0^x\int_0^{\frac{\pi}{2}}\cdots\int_0^{\frac{\pi}{2}}\sum_{i=1}^{N/2}B_i e^{-\lambda_i t}d\theta_1\cdots d\theta_{N/2}dt$$
$$B_i = \left[(\lambda_i - s)\prod_{j=1}^{N/2}\left(\frac{A_j}{\lambda_j - s}\right)\right|_{s\to\lambda_i}$$
$$A_i = \frac{1}{\pi\sigma_{2i-2}\sigma_{2i-1}} \quad \lambda_i = \frac{\cos^2\theta_i}{2\sigma_{2i-2}^2} + \frac{\sin^2\theta_i}{2\sigma_{2i-1}^2}. \tag{35}$$

[21]Computationally, inverting moment generating functions formed through products of exponential random variables is the same as performing an Inverse Laplace Transform on a transfer function with a polynomial denominator.

[22]As long as the sigma values are sequenced in order of their magnitudes, the poles of the integrand in (48) remain unique throughout each dimension of the integration and complications arising from repeated roots are avoided when applying Cauchy's Residue Theorem.

Equation (35) is the CDF for X when the ADC resolution is even. Since the integrand of this expression is finite across all dimensions of θ, and the limits of integration are well defined, (35) is numerically well behaved. Through (35), we can numerically estimate the CDF of X and subsequently the ENOB yield of even resolution ADCs.

When the resolution of the ADC is an odd number of bits, however, the number of terms summed in X is odd. If we imagine constructing an ADC with odd number of bits by adding one bit to an even resolution ADC, we can treat (48) as the moment generating function for the even contribution. Using Cauchy's Residue Theorem to invert (48) and then convolving the resulting PDF with the PDF for eta_{N-1} to capture the extra bit, we obtain the PDF for X in the case of odd resolutions. Integrating this expression, we obtain the CDF of X as shown in (36)—where σ_{2i-2} is the i-th even σ from (45) including σ_0, σ_{2i-1} is i-th odd σ from (45), and $\sigma_{\mathrm{N}-1}$ denotes the unpaired value from (45).

$$\mathrm{F_X}(x) = \int_0^x\int_0^{\frac{\pi}{2}}\cdots\int_0^{\frac{\pi}{2}}\sum_{i=1}^{N/2}C_i e^{-\omega_i t}d\theta_1\cdots d\theta_{N/2}d\varphi dt$$
$$B_i = \left[(\lambda_i - s)\prod_{j=1}^{N/2}\left(\frac{A_j}{\lambda_j - s}\right)\right|_{s\to\lambda_i}$$
$$A_i = \frac{1}{\pi\sigma_{2i-2}\sigma_{2i-1}} \quad \lambda_i = \frac{\cos^2\theta_i}{2\sigma_{2i-2}^2} + \frac{\sin^2\theta_i}{2\sigma_{2i-1}^2}$$
$$C_i = B_i\sin\varphi\sqrt{\frac{2t}{\pi\sigma_{N-1}^2}} \quad \omega_i = \lambda_i\sin\varphi + \frac{\cos^2\varphi}{2\sigma_{N-1}^2}. \tag{36}$$

From a computational standpoint, the CDFs given by (35) and (36) are quite expensive, and the time required to numerically estimate the CDF for X with reasonable error becomes impractically large as the dimension of the integrals becomes large. Nevertheless, the CDFs given by (35) and (36) along with probability relationship given by (34) allow us to estimate the ENOB yield of a SAR ADC more efficiently than circuit level Monte-Carlo simulations. We provide a more convenient approximation for the CDFs given in (35) and (36) in Section V.

REFERENCES

[1] B. Murmann, "A/D converter trends: Power dissipation, scaling and digitally assisted architectures," in *Proc. IEEE Conf. Custom Integr. Circuits*, Sep. 21–24, 2008, pp. 105–112.

[2] Z. Zheng, U.-K. Moon, J. Steensgaard, B. Wang, and G. Temes, "Capacitor mismatch error cancellation technique for a successive approximation A/D converter," in *Proc. IEEE Int. Symp. Circuits Syst.*, Jul. 1999, vol. 2, pp. 326–329.

[3] B. Gregoire and U.-K. Moon, "Reducing the effects of component mismatch by using relative size information," in *Proc. IEEE Int. Symp. Circuits Syst.*, May 2008, pp. 512–515.

[4] M. Saberi, R. Lotfi, K. Mafinezhad, and W. A. Serdijn, "Analysis of power consumption and linearity in capacitive digital-to-analog converters used in successive approximation ADCs," *IEEE Trans. Circuits Syst. I, Reg. Papers*, vol. 58, no. 8, pp. 1736–1748, Aug. 2011.

[5] J. McNeill, K. Chan, M. Coln, C. David, and C. Brenneman, "All-digital background calibration of a successive approximation ADC using the 'split ADC' architecture," *IEEE Trans. Circuits Syst. I, Reg. Papers*, vol. 58, no. 10, pp. 2355–2365, Oct. 2011.

[6] S.-C. Lee and Y. Chiu, "Digital calibration of capacitor mismatch in sigma-delta modulators," *IEEE Trans. Circuits Syst. I, Reg. Papers*, vol. 58, no. 4, pp. 690–698, Apr. 2011.

[7] S. Weaver, B. Hershberg, P. Kurahashi, D. Knierim, and U.-K. Moon, "Stochastic flash analog-to-digital conversion," *IEEE Trans. Circuits Syst. I, Reg. Papers*, vol. 57, no. 11, pp. 2825–2833, Nov. 2010.
[8] Y.-Z. Lin, S.-J. Chang, Y.-T. Liu, C.-C. Liu, and G.-Y. Huang, "An asynchronous binary-search ADC architecture with a reduced comparator count," *IEEE Trans. Circuits Syst. I, Reg. Papers*, vol. 57, no. 8, pp. 1829–1837, Aug. 2010.
[9] K. R. Lakshmikumar, R. A. Hadaway, and M. A. Copeland, "Characterization and modeling of mismatch in MOS transistors for precision analog design," *IEEE J. Solid-State Circuits*, vol. SC-21, no. 6, pp. 1057–1066, Dec. 1986.
[10] A. Van den Bosch, M. Steyaert, and W. Sansen, "An accurate statistical yield model for CMOS current-steering D/A converters," in *Proc. IEEE Int. Symp. Circuits Syst.*, May 2000, vol. 4, pp. 105–108.
[11] Y. Cong and R. L. Geiger, "Formulation of INL and DNL yield estimation in current-steering D/A converters," in *Proc. IEEE Int. Symp. Circuits Syst.*, May 2002, pp. 149–152.
[12] M. Kosunen, J. Vankka, I. Teikari, and K. Halonen, "DNL and INLyield models for a current-steering D/A converter," in *Proc. IEEE Int. Symp. Circuits Syst.*, May 2003, pp. 969–972.
[13] G. I. Radulov, M. Heydenreich, R. W. van der Hofstad, J. A. Hegt, and A. H. M. van Roermund, "Brownian-bridge-based statistical analysis of the DAC INL caused by current mismatch," *IEEE Trans. Circuits Syst. II, Exp. Briefs*, vol. 54, no. 2, pp. 146–150, Feb. 2007.
[14] M. J. M. Pelgrom, A. C. J. Duinmaijer, and A. P. G. Welbers, "Matching properties of MOS transistors," *IEEE J. Solid-State Circuits*, vol. 24, no. 5, pp. 1433–1439, Oct. 1989.
[15] S. Kuboki, K. Kato, N. Miyakawa, and K. Matsubara, "Nonlinearity analysis of resistor string A/D converters," *IEEE Trans. Circuits Syst.*, vol. CAS-29, no. 6, pp. 383–390, Jun. 1982.
[16] M. J. M. Pelgrom, A. C. J. V. Rens, M. Vertregt, and M. B. Dijkstra, "A 25-Ms/s 8-bit CMOS A/D converter for embedded application," *IEEE J. Solid-State Circuits*, vol. 29, no. 8, pp. 879–886, Aug. 1994.
[17] A. Moschitta and D. Petri, "Stochastic properties of quantization noise in memoryless convertors affected integral nonlinearity," *IEEE Trans. Instrum. Meas.*, vol. 53, no. 4, pp. 1179–1183, Aug. 2004.
[18] R. van de Plassche, *CMOS Integrated Analog-to-Digital and Digital-to-Analog Convertors*. Boston, MA: Kluwer Academic, 2003.
[19] W. Kester, *The Data Conversion Handbook*. New York: Newnes, 2005.
[20] Y. Cong and R. L. Geiger, "Switching sequence optimization for gradient error compensation in thermometer-decoded DAC arrays," *IEEE Trans. Circuits Syst. II, Analog Digit. Signal Process*, vol. 47, no. 7, pp. 585–595, Jul. 2000.
[21] J. A. Gubener, *Probability and Random Processes for Electrical and Computer Engineers*. New York: Cambridge Univ. Press, 2006.
[22] R. B. Davies, "The distribution of a linear combination of chi-squared random variables," *J. Royal Stat. Soc. C, Appl. Stat.*, vol. 29, pp. 323–333, 1980.
[23] P. G. Moschopoulos and W. B. Canada, "The distribution functions of a linear combination of the chi-squares," *Comput. Math. Appl.*, vol. 10, no. 4/5, pp. 383–386, 1984.
[24] B. Murmann, (2010) EE315B VLSI Conversion Circuits [Online]. Available: https://ccnet.stanford.edu/cgi-bin/course.cgi?cc=ee315b&action=handout_download&handout_id=ID125185307612754

Jeffrey A. Fredenburg (S'08) received the B.S.E. and M.S.E. degrees in electrical engineering from the University of Michigan, Ann Arbor, in 2008 and 2010, respectively. He is currently working toward the Ph.D. degree at the University of Michigan, Ann Arbor.

Michael P. Flynn (S'92–M'95–SM'98) received the Ph.D. degree from Carnegie Mellon University, Pittsburgh, PA, in 1995.

From 1988 to 1991, he was with the National Microelectronics Research Centre, Cork, Ireland. He was with National Semiconductor, Santa Clara, CA, from 1993 to 1995. From 1995 to 1997 he was a Member of Technical Staff with Texas Instruments, DSP R&D Lab, Dallas, TX. From 1997 to 2001, he was with Parthus Technologies, Cork. He joined the University of Michigan, Ann Arbor, in 2001, and is currently an Associate Professor. He is Thrust Leader responsible for Wireless Interfaces at Michigan's Wireless Integrated Microsystems NSF Engineering Research. His technical interests are in RF circuits, data conversion, serial transceivers and biomedical systems.

Dr. Flynn is a 2008 Guggenheim Fellow. He received the 2011 College of Engineering Education Excellence Award, the 2010 College of Engineering Ted Kennedy Family Team Excellence Award, and the 2005–2006 Outstanding Achievement Award from the Department of Electrical Engineering and Computer Science at the University of Michigan. He received the NSF Early Career Award in 2004. He received the 1992–1993 IEEE Solid-State Circuits Pre-Doctoral Fellowship. He is an Associate Editor of the IEEE JOURNAL OF SOLID-STATE CIRCUITS and serves on the Technical Program Committees of the International Solid State Circuits Conference (ISSCC). He previously served on the program committee of the Asian Solid-State Circuits Conference, and was Associate Editor of the IEEE TRANSACTIONS ON CIRCUITS AND SYSTEMS II from 2002 to 2004.